ACS Chemical Neuroscience
Cite This: ACS Chem. Neurosci. 2019, 10, 472−481
Research Article
pubs.acs.org/chemneuro

Huntingtin's N-Terminus Rearrangements in the Presence of Membranes: A Joint Spectroscopic and Computational Perspective

Geraldine R. Levy,[†] Koning Shen,[§,∥] Yulian Gavrilov,[‡] Pieter E. S. Smith,[†,⊥] Yaakov Levy,[‡] Rebecca Chan,[§] Judith Frydman,[§] and Lucio Frydman*[,†]

[†]Departments of Chemical and Biological Physics and [‡]Structural Biology, Weizmann Institute of Science, Rehovot 7610001, Israel
[§]Department of Biology, Stanford University, Stanford, California 94305, United States

Supporting Information

ABSTRACT: Huntington's disease is a neurodegenerative disorder resulting from an expanded polyglutamine (polyQ) repeat of the Huntingtin (Htt) protein. Affected tissues often contain aggregates of the N-terminal Htt exon 1 (Htt-Ex1) fragment. The N-terminal N17 domain proximal to the polyQ tract is key to enhance aggregation and modulate Htt toxicity. Htt-Ex1 is intrinsically disordered, yet it has been postulated that under physiological conditions membranes induce the N17 to adopt an α-helical structure, which then plays a key role in regulating Htt protein aggregation. The present study leverages the recently available assignment of NMR peaks in an N17Q17 construct, in order to provide a look into the changes occurring in vitro upon exposing this fragment to various brain extract fragments as well as to synthetic bilayers. Residue-specific changes were observed by 3D HNCO NMR, whose nature was further clarified with ancillary CD and aggregation studies, as well as with molecular dynamic calculations. From this combination of measurements and computations, a unified picture emerges, whereby transient structures consisting of α-helices spanning a fraction of the N17 residues form during N17Q17−membrane interactions. These interactions are fairly dynamic, but they qualitatively mimic more rigid variants that have been discussed in the literature. The nature of these interactions and their potential influence on the aggregation process of these kinds of constructs under physiological conditions are briefly assessed.

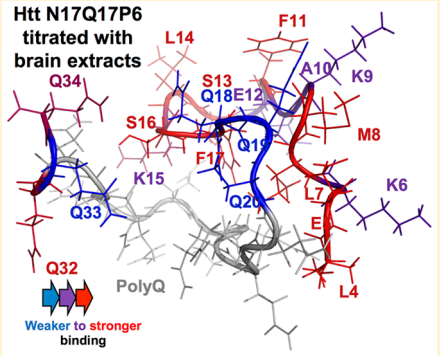

KEYWORDS: *Huntingtin, NMR spectroscopy, N17Q17 Htt-terminus, membrane-N17Q17 interactions, transient α-helical structures, Exon-1 folding landscape*

INTRODUCTION

Huntington's disease (HD) is an inherited neurodegenerative condition characterized by chorea, behavioral abnormalities, and brain atrophy.[1,2] HD is marked by the accumulation of amyloid aggregates in the brain,[3] consisting of a mutated form of the protein Huntingtin (Htt). Htt is a ubiquitously expressed, 350 kDa protein whose function is not fully understood, but which is known to be implicated in transcription regulation, vesicular transport, and neurogenesis.[4−8] The Htt mutation leading to HD involves an extended polyglutamine ("polyQ") tract in the first exon of the protein,[9] whose length is correlated with Htt's aggregation propensity in vitro and in vivo, as well as with the severity of the disease.[10] PolyQ length in unaffected individuals ranges between 6 and 17, yet exceeding a threshold of 37 glutamine residues leads to clinical pathogenicity. Strikingly, this Q-length is also a threshold for aggregation in vitro,[10] highlighting the correspondence between Htt's in vitro and in vivo aggregation and toxicity. In affected neurons, HD aggregates are primarily formed by a truncated N-terminal form of Htt, often comprising only the first exon of Htt, which contains the polyQ tract.[11−14] Studies of this exon1 fragment of Htt (Htt-Ex1) have proven relevant to disease phenotypes, as it appears that Htt-Ex1 actually accumulates in affected neurons and becomes a major component of the neuronal aggregates.

Htt-Ex1's polyQ tract is flanked by a short N-terminal domain, called N17, and a short C-terminal proline-rich tract (Figure 1). Recent studies have highlighted the important

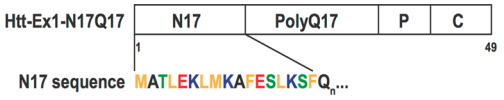

Figure 1. Domain structure of Htt-Ex1 illustrated for N17Q17. N17, N-terminal domain; polyQ, poly-Gln tract; P, Pro-rich region with six proline residues; C, short C-terminal linker region and hexahistidine tag. N17 sequence properties: gold, hydrophobic; red, negatively charged; blue, positively charged; green, polar Ser/Thr. In the present study, the construct included 17 glutamine residues, in order to temper the aggregation process and the NMR peak overcrowding arising for longer polyQs.

Received: July 14, 2018
Accepted: August 27, 2018
Published: August 27, 2018

DOI: 10.1021/acschemneuro.8b00353
ACS Chem. Neurosci. 2019, 10, 472−481

contribution of these flanking domains to Htt's conformation, aggregation, and toxicity. In particular, many studies have noted the pivotal role that the so-called N17 domain, the N-terminal first 17 residues, has in promoting Htt's aggregation.[15−21] N17 not only promotes formation of early stage intermediates that rapidly enhance the rate of Htt aggregation, but is also a site of interaction with cellular factors that modulate Htt's aggregation and toxicity.[14,22,23] These include post-translational modification factors[14,22,23] such as phosphorylation[22,24] and SUMOylation,[25] as well as the chaperone TRiC/CCT,[18] and possibly Hsp70.[26] The mechanism by which N17 regulates Htt conformation, cellular interactions and overall function has remained elusive, and therefore remains a topic of active investigation. Htt-Ex1 is itself largely unstructured, but it aggregates with a structured beta spine conformation akin to those arising in other amyloid diseases.[3] Solid-state NMR studies of an N-terminal fragment of Htt showed that N17 is helical in amyloid fibrils;[16,27−31] solid state NMR and biochemical studies have suggested that there may be distinct polyQ folding motifs, proximate in space.[38,39] Still, it is increasingly suspected that these amyloid aggregates have a protective, rather than toxic function.[32] In cultures of neuronal cells, formation of Htt-inclusion bodies lowers the risk of death, suggesting that the inclusion body itself is protective,[32] or that only certain types of inclusions are toxic.[33,34] Furthermore, an HD mouse model forms many inclusion bodies but exhibits no neuronal dysfunction.[35] This has led to the idea that other aberrant species are linked to neuronal toxicity, including monomeric or oligomeric polyQ-expanded Htt species.[36−38] These so-called prefibrillar intermediates have been the subject of extensive studies,[36−38] yet understanding the nature of these soluble Htt species and how they contribute to pathological mechanisms has remained challenging, largely due to their transient and dynamic nature, that has made these fragments refractory to conventional structural biology approaches.

High-resolution NMR could be highly informative to unravel the nature of these monomeric and oligomeric fragments, yet such studies are challenging. A recent communication demonstrated their usefulness in a short polyQ construct, by analyzing changes observed in its CEST NMR and EPR spectra upon titrating it with lipids in ca. 1:2 ratios.[39] Obtaining the assignments required for a comprehensive solution NMR investigation of longer polyQ constructs requires dealing with a large number of very similar residues present in the homopolymeric polyQ segment, and with a high degree of mobility and disorder which reduces the chemical shift dispersion of the N-terminal fragment, and broadens the spectral lines of the amide protons by exposing them to a rapid exchange with water. We recently managed to overcome these challenges for a Htt-Ex1 variant containing N17; a Q17 polyQ tract; a short region of six prolines, followed by a His_6 purification tag (herein Htt N17Q17). For this domain, which produces fibrillar Thio-T-positive aggregates at 100 μM and can seed aggregation of Htt-Ex1-Q50, the methodological NMR difficulties mentioned above could be alleviated by (i) using suitable pH and temperature ranges to slow down hydrogen exchange, and (ii) relying on a portfolio of high-field 3D, 4D, and 5D NMR experiments capable of separating even very closely spaced resonances. Using such strategies we succeeded in assigning the non-proline backbone ^{13}C and ^{15}N and several side-chain ^{13}C resonances, for the 49-residue Htt N17Q17.[40] This atomic level information is here leveraged to explore how this construct interacts with cellular and cellular-like components. Toward this end, NMR spectra were titrated with different fractions arising from brain extracts, revealing site-specific changes when the titrations involved membrane-containing components. To further clarify the meaning of these changes, experiments were repeated upon titration with small unilamellar vesicles (SUVs) mimicking large membrane components; the site-specific changes were then qualitatively recapitulated, even if at much lower membrane/Htt ratios. The driving force of these site-specific changes was sought utilizing biochemical assays, and further clarified utilizing computational (MD) simulations. The latter suggested that the fully disordered N17Q17 forms transient α-helical structures throughout parts of the polypeptide, in agreement with previously conducted computations on the N17 fragment and with the 3D HNCO data that we observe. The consequences that these integrated computational and experimental approaches provide on the interplay between the transient conformations that N17Q17 will adopt in the presence of brain components and the propensity of Htt to form aggregates, are briefly discussed.

RESULTS AND DISCUSSION

Solution NMR Evidence of Residue-Specific Interactions with Membrane-Containing Environments. Since Htt exerts its deleterious effects in neuronal tissues, we sought to characterize cellular interactions of Htt, by incubation of N17Q17 with mouse brain extract (BE). The most evident change observed upon titrating N17Q17 with BE is the disappearance of certain peaks in the corresponding NMR spectra. Figure 2 illustrates this with representative 2D projections ($^{13}C/^{15}N$, $^{13}C/^{1}H$, $^{1}H/^{15}N$) taken out of a series of BEST-HNCO 3D data sets recorded for increasing concen-

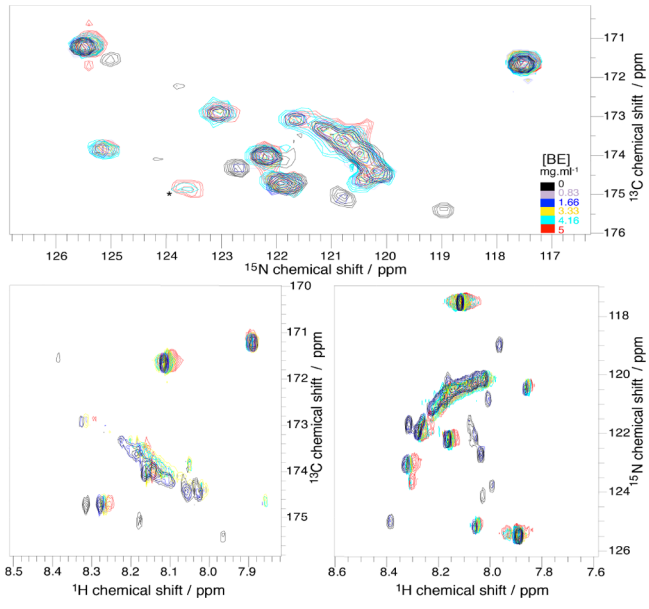

Figure 2. Superimposed projections (partial regions) arising from a series of 3D HNCO spectra collected on a N17Q17 fragment, as a function of different concentrations of brain extract (BE) externally added to the peptide solution. Indicated with an asterisk is a resonance arising from the BE itself. All measurements were performed at 20 °C and pH 7.2 on a 180 μM protein solution, on a cryoprobe-equipped 800 MHz NMR spectrometer.

DOI: 10.1021/acschemneuro.8b00353
ACS Chem. Neurosci. 2019, 10, 472−481

trations of unfractionated BE. Notice that the changes in chemical shifts are relatively minor, yet the differential changes in line widths (and thereby in peak intensities) are easily observable. Similar resonance/residue-specific changes, noticeable in the intensities but weak in chemical shift displacements, are also observed in 2D $^{13}C/^{1}H$ HSQC BE titration experiments when focusing on the side chain resonances (Supporting Information Figure S1). In order to better appreciate these changes, Figure 3A illustrates how the

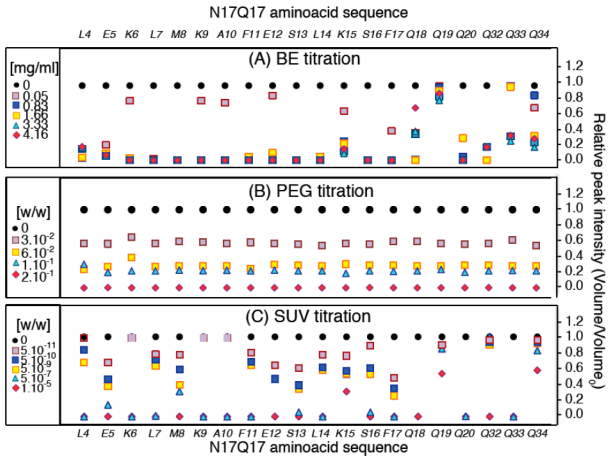

Figure 3. Changes in the relative peak intensity ratios identified for different N17Q17 residues in HNCO experiments, when titrated by (A) raw brain extracts, (B) PEG, a crowding mimicking agent, and (C) small unilamellar vesicles, mimicking a membrane environment. All measurements were done at 10 °C and pH 7.2 using urea as internal standard added for the sake of uniform quantitation.

normalized 3D peak volumes that each of the backbone amide peaks exhibits, varies as a function of increasing BE concentration. Notice that this graph only describes the changes for the N17Q17 residues that can be unambiguously identified under neutral pH and 10 °C; notice as well that peak intensities in these (and throughout the remaining) titrations were normalized to a common scale using an external reference ($^{13}C/^{15}N$-urea) whose HNCO peak intensity was found indifferent to the titrants. We ascribe the progressive disappearance of the Htt peaks that these results evidence to the peptide's binding to large macromolecular components present in the BEs. The slow rotational tumbling of such macromolecular binding would be associated with a progressive line broadening of the peptide peaks, which would make these increasingly difficult to detect by the HNCO 3D acquisitions. It is interesting to contrast this behavior with that observed when exposing N17Q17 to PEG, a commonly used crowding agent. Also the addition of this macromolecule promotes a decrease in the Htt peak intensity (Figure 3B), but suitable renormalization makes it clear that the decrease is not residue specific, but rather affects the correlation tumbling time of the peptide as a whole. It is also interesting to contrast this behavior to that observed by NMR for shorter N17-polyQ constructs when titrated with lipid-based micellar nanoparticles, where much smaller signal intensity changes are seen for the peptides, even at considerably higher lipid/peptide ratios.[39] To further clarify the origin of the changes observed upon titrating Htt with BEs, the latter were fractionated through sequential centrifugation steps into a number of components—ranging from large membranes and organelles to soluble protein solutions. 3D HNCO experiments performed upon titrating Htt with various amounts of these fractions showed that, apart from an overall increased affinity for the larger cellular components, qualitatively similar spectra were obtained in the presence or absence of the soluble protein components (see Figure S2 for a summary of these results). The membrane-rich fractions led to the disappearance of specific residues, in a behavior reminiscent of that seen upon titrating with intact BEs. By contrast, experiments performed in buffer solutions led to minor, attenuations in signal. In view of this, titrations were repeated using membrane-like structures; these were mimicked by relying on SUVs,[41] vesicles that could then serve to assess Htt-membrane interactions at precisely known micellar/protein ratios. As in the BE case, addition of SUV led to negligible changes in the peak positions ($\Delta\delta \approx 0.06$ ppm for ^{1}Hs; $\Delta\delta \approx 0.6$ ppm for ^{13}C or ^{15}N). Instead, SUVs led to dramatic and concentration-dependent decreases in the residues' peak intensities even at ppb w/w concentrations. Figure 3C illustrates representative results of these titration experiments. Clearly, as in the case of the BE titrations, the effects of the SUVs are not uniform, and affect certain residues more strongly than others. To a large extent these changes are akin to those reported on the binding of another intrinsically disordered neurodegeneration-linked protein to SUVs.[42]

In an effort to place this binding specificity in a framework affording a more quantitative measure of each residue's binding affinity, we assayed to represent it as a simple association whereby numerous peptide residues can interact with the larger SUV particle. Thus, the binding of a particular peptide residue P to the macromolecular (e.g., SUV) substrate S, was represented by an equilibrium

$$P_nS \Leftrightarrow nP + S \tag{1a}$$

which will be defined by a dissociation constant

$$\begin{aligned} K_d &= \frac{[P]^n[S]}{[P_nS]} \\ &= \frac{[P]^n([S_0] - [P_nS])}{[P_nS]} \\ &= \frac{[P]^n\{[S_0] - ([P_0] - n[P])\}}{([P_0] - n[P])} \end{aligned} \tag{1b}$$

where K_d reflects the ratio between the concentration of the various species, $[S]_0$ and $[P]_0$ are the (known within a scaling constant) initial concentration of SUV and protein added, and $[P]$ is the concentration of free residue, which can be estimated from the relative NMR peak intensity under the assumption that the bound "P_nS" species will be invisible in the NMR due to the large sizes of the SUVs. Although eq 1 should provide a description of a residue's relative binding affinity vis-à-vis, the affinities of other residues in the construct, no fitting algorithm provided reasonable parameters for the K_d and n values, neither for the BE nor for the SUV titration experiments. That this will be the case for the latter can be appreciated by the fact that, although extremely low [SUV] concentrations suffice to affect substantially most residues' signals, these concentrations need to be increased by orders of magnitude, in order to effect further changes. This inconsistency probably means a change in the nature of the binding with increasing SUV concentration; for instance a change from an SUV-catalyzed but Htt/Htt-dominated binding interaction, to an SUV/Htt-

DOI: 10.1021/acschemneuro.8b00353
ACS Chem. Neurosci. 2019, 10, 472−481

dominated binding interaction. Alternatively, the log-like nature of the changes observed could reflect the elimination of distortions in the SUV structure as its ratio to the protein concentration increases. Still, given the clear message of site specificity being conveyed by the NMR, we decided to qualitatively describe the binding affinity of Htt's residues by describing, for each residue observed in these titrations, the [SUV] or [BE] required to bring the intensity of its NMR peak down by 50%. The results of such fits are summarized in Figure 4. Notice that although the quantitative values

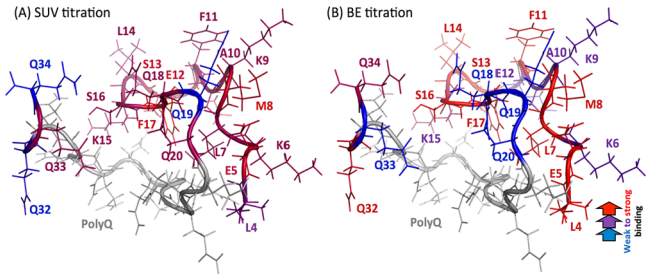

Figure 4. Color-coded residue dependence of binding interactions with (A) SUV and (B) brain extracts, as derived from an analysis of the HNCO NMR titrations as described in the text. Grayed residues correspond to unassigned backbone positions.

associated with each residue do not necessarily reflect a well-defined dissociation process like that given in eq 1, nor one whose thermodynamic parameters can be univocally defined, they serve to highlight the residue-by-residue specificity of the Htt binding vis-à-vis the two titrating entities. Interesting and important to note then are the parallelisms observed for the behaviors of the various residues, particularly the faster attenuation experienced by residues in the edge of the N17 fragment, in both sets of titration experiments.

The Influence of SUVs on Htt's Secondary Structure and Aggregation Propensity. As complement to these NMR studies, we tested the impact of the SUVs on the aggregation propensity and the secondary structure displayed by the N17Q17. Htt aggregation kinetics were measured by ThioflavinT (ThT; Figure 5A).[21] Addition of SUVs in the concentration range observed to fully bind N17Q17 by NMR had a negligible effect on the kinetics of aggregation and, if anything, it slightly retarded formation of ThT-binding species. Similar results were observed using a pathogenic length Htt-Exon1 with a Q51 tract (Figure S5). Circular dichroism analyses of N17Q17 were consistent with a molten globule structure. Analysis of the N17Q17 CD spectra in the absence of SUVs with the K2D3 neural network analysis algorithm indicated an ~5% helical and ~20% β-sheet content with 75% disorder. Addition of SUVs followed by immediate analysis produced a slight but clear alteration in secondary structure (Figure 5B). Compared to Htt in buffer, addition of the SUVs increases in helical content as measured by changes in elipticity at 222 nm (Figure 5C) and by analysis with the K2D3 algorithm (Figure 5D).[43] These changes are time dependent, and over the course of hours evidence a decrease in α−helicity; presumably reflecting the onset of Htt oligomerization (Figure S7).

MD Sheds Light on the Experimental Changes Observed upon Titrating N17Q17 with Bilayers. In a recent study, the chemical shift values arising from a variety of multidimensional NMR experiments were used in order to

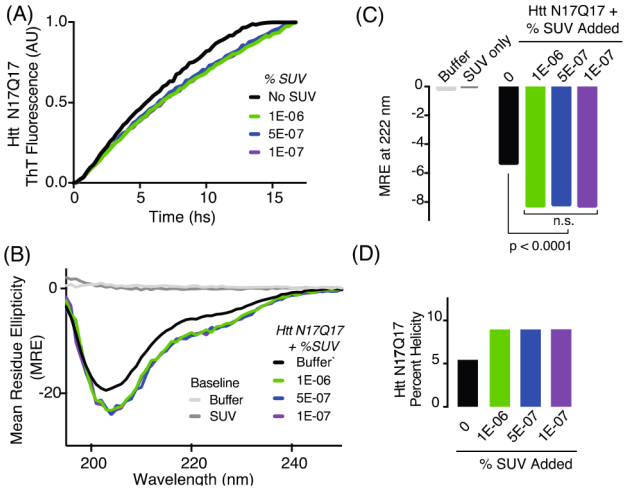

Figure 5. Effect of SUVs on N17Q17 aggregation kinetics and secondary structure. (A) Normalized aggregation kinetics of 20 μM N17Q17 measured using ThT fluorescence in the absence or presence of the indicated SUV concentrations (%w/w). (B) CD spectra recorded for 20 μM N17Q17 in the absence or presence of the indicated concentrations of SUVs. Baseline readings of Buffer −/+0.01% SUV also shown. (C) Impact of SUVs on the MRE values at 222 nm of the N17Q17 CD spectra. (D) Helicity for N17Q17 in the absence or presence of SUVs calculated using the K2D3 algorithm for CD-based predictions of secondary structure.

derive structural information regarding the N17Q17 construct used in this study. Computation predictors applied to that data coincided in concluding that at low pH, a central region (Ala10-Gln22) of the construct possesses a significant α-helical secondary structure propensity. However, this feature disappears for the neutral pH environments used in the present study. Furthermore, while the titrations in Figures 3 and 4 significantly changed the intensities of backbone resonances, barely any changes in the backbone's (or for that matter in the side chain's) chemical shifts were noticed along any of the interrogated dimensions. Hence one can conclude that, despite the residue specificity highlighted in the previous paragraph, exposing N17Q17 to membranes or to membrane-containing BEs introduces at most a subtle change in the otherwise largely disordered structure adopted by the protein in solution—at least judging by the "free" fraction [P] that is detectable by NMR. This analysis is fully consistent with the CD measurements just presented. Yet it is also clear that, unlike the situation observed in titrations with PEG, there is a residue specific change triggered by the addition of BEs and SUVs to Htt N17Q17. While CD measurements suggest a slight increase in α-helical content, these measurements cannot provide detailed structural insight into this change. In order to investigate what is the structural meaning of this specificity, a series of independent MD calculations were carried out. We refer to these as "independent" calculations to reflect the fact that no residue-specific information arising from the NMR data was used as input or constraint for these simulations. Instead, the sole input extracted from these experiments and utilized in order to guide the MD calculations, was the global observation that NMR detected a site-specific, discriminating and attractive interaction between the zwitterionic surfaces exposed by SUVs and the Htt peptide. Discriminating, in the sense that it did not erase the NMR signatures of all residues simultaneously; and attractive, in the sense that the binding of the peptide to the

DOI: 10.1021/acschemneuro.8b00353
ACS Chem. Neurosci. 2019, 10, 472−481

slowly tumbling membrane-like structures, did eventually impart on the former the particles' long correlation time. Furthermore, these simulations were designed to provide a qualitative microscopic insight on the changes evidenced by the NMR spectra, and hence its membranes were modeled for simplicity as beads based on Ar atoms. Also assumed in these MD simulations (see Methods for further details) were: (i) ROSETTA-derived initial peptide conformations according to what we had previously observed for N17Q17 at neutral pH; (ii) water molecules; (iii) membranes that were mimicked by two flat, extended square surfaces: an upper one that although neutral overall possesses alternating fractional charges centered at periodic lattice sites; and a lower one that is fully neutral and mimicked the membrane's hydrophobic core. Under these conditions the MD runs revealed, after consistent runs converging in about 300 ns, that moderate attractive interactions between the peptide and membrane could be observed when the latter was endowed with small (<0.1) fractional charges: larger charge values would reflect in an immediate collapse of the peptide onto the synthetic membrane surface, whereas if fully neutral, membranes actually repulsed the Htt peptide. The rationale for considering small, alternating fractional charges reflects the possibility that the polar heads in the vesicles seeking to interact with the Htt, be shielded by counterions present in the medium. This guided our choice for the upper, zwitterionic lattice layer onto a ... −0.05/0/+0.05/0/−0.05... alternation. With this choice, a clearly very dynamic picture of the peptide-membrane interaction emerged; Videos S1 and S2 give an idea of this for initial N17Q17 structures in the presence and absence of a membrane. As these runs also evidence, a significant helicity repeatedly emerges between residues 3−10 of the peptide. Figure 6A illustrates this with 3 prototypical structures arising upon averaging simulations over 300 ns assuming different initial conditions; Figure 6B further describes this with the average helicity of each residue in the polypeptide. Despite the qualitative nature of these simulations, energy-based considerations (Figure 6C) reveal that these structures arise due to interactions between the weakly charged membrane and certain charged and neutral residues partaking of the peptide N17 fragment, particularly Met_1, Leu_4, Leu_7, Met_8, Phe_{11}, and Leu_{14}; a significant interaction is also measured close to the His tag for Leu_{41}. This is in accordance with our CD measurements as well as with previous theoretical and experimental reports,[44,45] which give evidence of a helical region emerging in Htt interacting with membranes as a result of N17's amphipathic nature. As shown by the structures in Figure 6, the membrane-facing side of this helix is mostly formed by hydrophobic residues, while charged residues (Glu_5, Lys_6, Lys_9, Glu_{12}, Lys_{15}) form the helix's opposite side. These analyses also reveal substantial conformational dynamics remaining in the residue; however, this is much reduced over what the same simulations predict for the peptide in absence of the membrane. This is summarized in Figure 6D, which indicate that helical N17 conformations span more residues and are formed more rapidly when the peptide interacts with membranes. These membrane-less predictions are also in agreement with those described by Zhang et al. for the isolated N17 peptide.[45]

CONCLUSIONS

Ex1's N17 fragment can deeply affect and modulate the aggregation propensity of the proximal polyQ tract.[18,19,21,46]

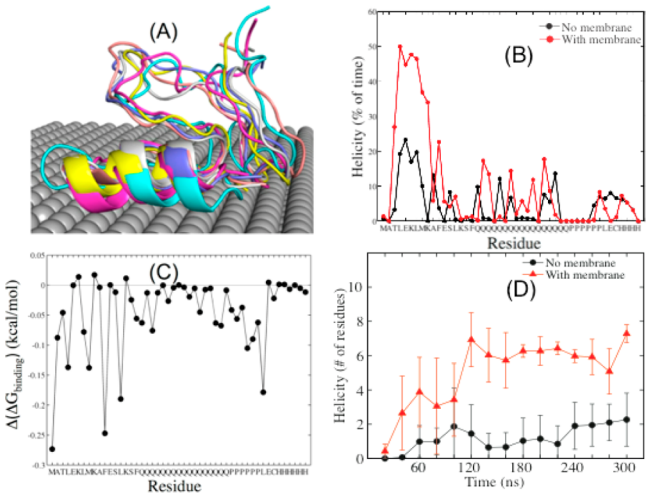

Figure 6. MD calculation of the Htt-membrane interaction. (A) Representative conformations of Htt interacting with a coarse-grained membrane, parametrized on the basis of a fractionally charged upper layer and a lower neutral layer. (B) Averaged helicity characterizing each residue in the analyzed peptide over its ensemble of conformations, in the presence and absence of the model membrane. (C) Computationally estimated free energies associated with the Htt binding to the coarse-grained membrane ($\Delta\Delta G_{binding}$, kcal/mol). The figure represents the average values from three 300 ns runs. (D) Time evolution predicted for the system in the presence and absence of the membrane. Error bars represent deviations arising from multiple runs; notice the larger number of residues with helical propensity arising upon establishing the interactions. See Supporting Information Videos S3 and S4 for further insight.

The intrinsically disordered nature of N17 in physiological solutions, however, raises questions regarding the structural mechanism underlying this modulation. The conditions in the cell could affect this process through interactions with cellular components. Given the interactions that have been documented between Htt-Ex1 N-terminal domain and vesicles, the endoplasmic reticulum (ER) and mitochondria,[47−50] cellular membranes are natural starting points for such potential structural changes. Driven by this possibility, changes in both the N17 and the various polyQ constructs upon being exposed to membrane-like components, have been investigated in recent years by theoretical and experimental means.[39,44,45,51−55] These investigations extended to mutant Htt Ex1 and peptide derived fragments, which were shown to increase binding to numerous phospholipids, in both Q-length and bilayer-dependent manners.[51,52] Isolated N17 fragments exposed to micellar mixtures were found to gain a helical propensity, with side chains of its hydrophobic residues oriented toward the hydrophobic core of the micelles.[56] This formation of an α-helical structure by the N17 terminus has been suggested to arise with the onset of amphiphilic peptide-membrane interactions.[31] Studies on the anchoring of just the N17 peptide to a POPC bilayer have also been done using all-atom molecular dynamics, which showed that this fragment became largely α-helical, particularly from residues 7 to 16.[44] This was rationalized as part of a membrane-anchoring mechanism involving nonpolar residues, as well as the putative formation of hydrogen bond or salt-bridges with the phosphate group of the phospholipids. Tryptophan fluorescence results also supported this, while indicating a penetration into the bilayer of the first residue of Htt.[53] Experimental evidence for the formation of this structure upon exposure to lipids also

DOI: 10.1021/acschemneuro.8b00353
ACS Chem. Neurosci. 2019, 10, 472−481

comes from recent CEST NMR measurements, even given the orders-of-magnitude differences in the lipid concentrations assayed and the different structure of such study's construct.[39]

The present study attempted to shed further light into these changes utilizing a multipronged experimental/computational approach. Yet unlike what is commonly done, the former was not utilized as starting point of the latter, apart from the conceptually soft imposition of requiring the reproduction of a residue-specific attraction between the peptide and the modeled membrane. The NMR and MD can thus be seen as parallel approaches, and it is thus interesting to evaluate the pictures emerging from these complementary methods. Modeling a simplified bilayer so as to fulfill the imposition mentioned above, showed that interacting N17Q17 units transitioned from a largely disordered and dynamic structure, to a more ordered one. The rise in structural features is evidenced by the changes in numerous indicators (Figure 6); still, the MD runs reveal the presence of high residual dynamics transforming the helices into disordered peptides, something that would explain the absence of systematic NMR chemical shift changes upon titration. The exact degree of order induced by the addition of the membrane, however, cannot be assessed from our MD runs, that lack the sophistication of more involved models.[57] Another feature on which our experiments and computations independently concur, concerns the location of the structural changes arising when the peptide interacts with membranes. In both cases, amino acids belonging to N17 are involved, with a relatively weaker interaction of the polyQ region. Indeed, other reports show that the N17 residues flanking the polyQ region are crucial in polyQ association with membranes.[58,59] In our study, we observe an exact match between experiments and calculations are thus seen for the behavior of residues 4, 7, 11, 14, and 15, and a partial match for residues 6, 8−10, 12, and 13, and for the 17 glutamine residues of the polyQ. While the kind of NMR experiments that were here presented cannot reveal the nature of these structural changes, the MD ascribes these to the formation of transient α-helices. This agrees well with our CD measurements and with the residue-specific solid-state NMR and the all atom simulations that have been performed on the N17 residues,[47−50] even if the extent and the stability of the α-helical structures that we observe are slightly more restricted and lower.

Interesting as well are the differences between the α-helices that arise upon exposing the peptide to membranes, and the N17Q17 structures observed by lowering the pH of the solution.[40] The latter exhibited a much higher helical propensity, which also extended over a more extensive region of the peptide than what is indicated by Figures 3−5. That strong conformational pH effect was interpreted purely in terms of electrostatics upon decreasing protonation,[40] while the structural transitions reported here upon introducing a bilayer seem to be driven by a combination of hydrophobic and electrostatic interactions, which may be more amenable for seeding protein aggregation. In both cases, however, a unified picture emerges whereby the N17 fragment is disordered, yet on the threshold of adopting an α-helical structure. This is a transition that can then occur if prompted by a number of different environmental changes: slightly charged, zwitterionic membranes can trigger such transition. The ensuing transient structures have limited lifetimes and do not appear to extend deeply into the polyQ chain, but they may be sufficient for affecting aggregation. The extent of this process under physiologically relevant conditions, however, remains to be defined. At the SUV concentrations explored in this NMR study (0.6−650 nM), the variations induced in N17Q17's helical propensities did not appear to enhance aggregation; this was the case for both N17Q17 and N17Q51 Htt constructs. Still, we note that, at much higher SUV concentrations (6−130 μM), the previously reported increase in aggregation kinetics[55] was also observed (Figure S6). This suggests that membrane-binding will induce conformational transitions in Htt and will also impact Htt's aggregation. The question that arises is whether these two processes are related to one another. Indeed, although the tendency of N17 to adopt an α-helical structure has been now observed in several constructs and detected by independent means,[49,60] it is unclear how or even if this propensity acts at a molecular level, to modulate Htt's aggregation.[40] On one hand it has been argued that transitioning from a disordered to a partly ordered structure could discourage "cross-talk" between the ordered N17 and the more mobile polyQ portions of the peptide, thereby preventing aggregation.[31,61,62] On the other hand it has been postulated that the N17 α-helical propensity leads to an amphipathic character, which promotes promiscuous interactions with other Htt fragments and thereby accelerates Htt's aggregation. It remains to be seen which of these options dominates under relevant *in cell* conditions. It also remains to be seen how this N17-localized feature is preserved upon elongating the polyQ$_n$ chain toward $n \approx 35-40$ aggregation threshold, and whether it is enhanced, preserved or suppressed by post-translational modifications which include phosphorylations of the two serines in the N17 segment or acetylation, which has also been shown to affect lipid binding.[63] It also remains to be assessed if these structural changes act as triggers for various molecular interactions involving chaperones or other cellular mechanisms of protein quality control, and how the local changes mentioned above modulate the transport of monomers and oligomers throughout the various cellular compartments. We are currently pursuing these efforts using combinations of native and mutated Ex1 targets, using NMR experiments that focus on both the backbone and the side-chain resonances, via relaxation-dispersion NMR experiments,[64] as well as by a variety of complementary biochemical and computational tools.

METHODS

Protein Preparation. The fragment illustrated in Figure 1, henceforth N17Q17, was isotopically labeled by overexpression in a Nico *E. coli* BL21 strain. This was achieved by growing cells in M9 minimal media and salts (12.8 g/L of Na_2HPO_4, 3 g/L of KH_2PO_4, 0.5 g of NaCl, 1 mM $MgSO_4$, 50 μM $CaCl_2$, ammonium chloride (1 g/L), 0.4% (w/v) D-glucose) in glass-distilled, autoclaved H_2O. For ^{15}N-labeling, $^{15}NH_4Cl$ was used; for $^{15}N-^{13}C-^{2}H$-labeling, $^{13}C-^{2}H_7$−glucose was used as well. Cultures of cells inoculated with the plasmid coding for N17Q17 were prepared in this media, diluted 40-fold in Lysogenic broth, and growth overnight to an OD_{600} of 0.6 at 37 °C. Thereafter, expression was induced with 1 mM IPTG for 4h at 37 °C. Cells were harvested by spinning at 4000*g* for 20 min at 4 °C; pellets were washed with PBS, recentrifuged prior to snap-freeze in liquid nitrogen, and stored at −80 °C. These were resuspended in 50 mM K-Hepes/pH 7.4, 20 mM Imidazole, 8 M GuHCl, sonicated three times for 1 min in ice, and incubated at room temperature for 30 min. The crude lysates were centrifuged at 18 000 rpm for 30 min at 4 °C, and the supernatant was loaded into a Ni-Sepharose column (GE) that had been previously charged and washed to baseline UV absorbance. The bound protein was then eluted using a 20−500 mM imidazole gradient in a buffer that

DOI: 10.1021/acschemneuro.8b00353
ACS Chem. Neurosci. 2019, 10, 472−481

included 50 mM K-Hepes (pH 7.4, no guanidine). The eluted fractions were monitored for the presence of protein by U.V. absorbance spectrometry at OD_{280}, and for the presence of protein with molecular weight consistent for N17Q17 by 4−12% sodium dodecyl sulfate (SDS) polyacrylamide gel electrophoresis (PAGE). Protein was dialyzed against 50 mM ammonium formate (pH 3.5) three times for 3 h each. After dialysis, the protein solution was spun at 3000 rpm for 5 min to pellet any aggregates. The resulting supernatant was then snap-frozen, lyophilized, and stored at −20 °C.

NMR Samples. Protein samples were investigated by preparing 180 μM solutions in 50 mM sodium phosphate buffers (pH 7.4). 10% D_2O was added for locking, and 0.001% DSS for spectral referencing. In order to deal with sample preparation imperfections throughout the titration experiments performed, 50 μM [^{15}N−^{13}C]-urea and 0.5 μM methanol was added for normalization of the Htt peak intensity changes that were observed (the urea was judged to undergo negligible intensity changes in these titrations, judging by its ratio to the DSS peak). In addition, chaperone experiments were performed in 50 mM K-Hepes, pH 7.4, 300 mM NaCl, 5% glycerol, 1 mM DTT. In all cases, 330 μL final volumes of titrand + titrant were placed in 5 mm Shigemi tubes, and final pH values were determined using a meter within the tube before running the experiments.

The NMR spectra of the Htt samples were recorded under different titrant concentrations. These included polyethylene glycol (PEG-10000, SigmaAldrich) which was assessed as a crowding agent; small unilamellar vesicles (SUVs) assessed as membrane-like models; and a variety of fractionated brain tissue extracts (BEs). Added PEG and BEs are reported as w/v fractions, whereas the SUV concentration is reported as w/w fraction. PEG was used as received. SUVs were prepared at a 5:3:2 DOPE/DOPS/DOPC molar ratio (Avanti Polar Lipids) as chloroform solutions; this solvent was evaporated under a stream of nitrogen gas, dried under vacuum to yield a thin film, rehydrated with a 20 mM sodium Na_2HPO_4 pH = 7.0 buffer, vortexed, and subject to several freeze−thawing cycles and sonications until the mixture became clear. The size of the resulting micelles was measured by dynamic light scattering and ranged between 40 and 70 nm. SUVs were stored at a 1% (w/w) concentration, corresponding to about 13 mM. This was diluted to ranges of 130 nM to 0.65 pM for the NMR experiments, and 130 μM to 0.65 nM for the aggregation kinetics assays.

All animal procedures were carried in accordance with the guidelines for animal experimentation from the ethical committee of Stanford University; they were undertaken according to Stanford's regulatory bodies and AAALAC guidelines. Mice brain extracts were produced from 250 mg of tissue material; this tissue was first homogenized in 500 μL of phosphate buffer (pH 7.4) including EDTA, PMSF, antipain, and leupeptine using a Potter homogenizer spinning for 10 min at 4 °C, and then transferred in aliquots into Eppendorfs. The Potter homogenizer was cleaned with water and ethanol between samples, and all steps were performed on ice. These brain tissue samples were then aliquoted, snap frozen and stored at −80 °C until used. Further fractionation was done on these samples including ultra centrifugation at 1000g (10 min) to separate whole cells; 20 000g (20 min) to separate mitochondria/nuclei/cytoskeleton; and 150 000g (3 h) to extract microsomes and small vesicles; the remaining supernatant is assumed to contain all soluble proteins.[65] All titrations were repeated multiple times, and the normalized peak intensity changes reported below were found to agree throughout these repeated titrations with R^2 values better than 0.92.

NMR Experiments. Titration experiments were performed using a Bruker AVANCE III 800 MHz spectrometer equipped with a 5 mm TCI Cryprobe, or on a Bruker AVANCE III 600 MHz spectrometer equipped with a 5 mm Prodigy probe. The bulk of the data here presented relied on 3D HNCO acquisitions performed using the BEST (band-selective excitation short-transient) experiment, optimized for minimal perturbation of aliphatic and water ^{1}H spins.[66] 100 ms evolution time on both the ^{15}N and ^{13}C channels and ≈1000 total indirect-domain time points were collected; with 24 suitably phase-cycled scans this lead to experimental times of ∼4 h/titration point. Data were processed and analyzed using NMRPipe[67] and CCPN scripts, in order to extract 3D volume values at the pertinent ^{1}H, ^{13}C, and ^{15}N chemical shifts. These resonance positions were correlated with specific sites in the N17Q17 backbone based on the assignments we have recently reported for this construct. In order to pinpoint these sites, chemical shifts were referenced using the absolute ^{1}H frequency of the DSS signal by means of suitably setting the spectrometer's xCAR, yCAR, and zCAR values.

Aggregation Kinetics. Lyophilized HttQ17 was resuspended in 50 mM sodium phosphate, pH 7.0 to a final concentration of 20uM in the presence of carious concentrations of SUVs and 12.5uM ThioflavinT dye (Sigma-Aldrich, St. Louis, MO). Reactions were placed in Costar 96-well plates (black with clear flat bottom polystyrene) and the change in the ThT fluorescence signal with time was monitored using a plate reader (Tecan Infinite M1000, Tecan Systems, San Jose, CA). Plate reader conditions were 30 °C, 446 nm excitation, 490 nm emission, read every 15 min.

CD Spectroscopy. CD samples were prepared by incubating 20 uM Htt in the presence of various concentrations of SUVs in 50 mM sodium phosphate buffer, pH 7.0. Far UV CD spectra were recorded on an Aviv CD spectrometer model 62A DS at 25 °C. Quartz cuvettes with path lengths of 1 mm were used, and CD spectra were obtained by averaging five individual spectra recorded between 260 and 190 nm, with a bandwidth of 1 nm, an averaging time of 1 s, and a settling time of 0.33 s. Each value of CD signal intensity reported at 222 nm corresponds to the average of five measurements.

All-Atom Molecular Dynamics (MD) Calculations. To further understand the meaning of the NMR titrations, all-atom MD simulations were performed evaluating the potential interactions of Htt with membranes. These calculations took the full peptide that was studied, but assumed a coarse-grained representation of the membrane. This consisted of two square layers of beads (30 × 30 beads per 2D layer); the beads in the lower layer were not charged and mimicked the hydrophobic membrane portion, while beads in the upper layer were given an alternating ... positive/neutral/negative/neutral... electrostatic nature to mimic zwitterionic polar heads. In order to simplify the scaling of nonbonded interactions (see below) the beads were modeled based on Ar atoms (m_a = 39.948) with a low epsilon value for their Lennard−Jones potential (0.0274580 in CHARMM27 force field). The membrane was restricted in space and its atom coordinates were not updated in time, but peptide-membrane interactions were allowed to fold into the latter's periodic boundaries by using the triclinic box approach. All atom molecular dynamics simulations were then performed using GROMACS (Ver. 5.0.4) with the CHARMM27 force field.[68−71] The linear constraint solver (LINCS) algorithm was used to control bond lengths during the simulation.[72] No ions were added due to system neutrality, and N and C termini of the peptide were chosen to be neutral ($-NH_2$ and −COOH). For motion equations integration, the leapfrog algorithm was used (2 fs steps); a modified Berendsen thermostat[73] was used to control the temperature at 300 K. We used explicit water molecules using the extended simple point charge (SPC/E) model due to its realistic behavior.[74,75]

Initial conformations of the N17 portion of the peptide were based on the predictions that CS-ROSETTA made for the N17Q17 structure at low and neutral pH using Pymol (ver 1.7.0.5[76]). The Q17 portion was originally modeled in an extended conformation and was subject to a number of 100 ns simulations before the long simulations were collected. We found that the initial conformations sampled by the Q17 did not impact the final membrane-Htt results substantially−probably reflecting the weak interaction that the Q17 fragment showed with our model membrane. In the starting frame of the MD calculations the peptide was located above the center of the membrane at a distance of 10 Å, and the peptide conformation was relaxed using a steepest descent method of energy minimization. The peptide/membrane systems were equilibrated in two steps (100 ps/phase): the first one was conducted assuming an NVT ensemble, and the second an NPT ensemble. For scaling of nonbonded membrane interactions we used 100 ns runs (one run per each chosen value of the membrane bead charge with neutral/low pH based conformation of the N17Q17) and the final production runs were 300 ns long

DOI: 10.1021/acschemneuro.8b00353
ACS Chem. Neurosci. 2019, 10, 472−481

(three runs) for the system with a membrane and 300 ns long (three runs) for the system without a membrane. The peptide-membrane binding free energy was calculated using the g_mmpbsa tool, with the entropic term excluded from the free energy calculations due to its high standard error vis-à-vis other terms.[77] Furthermore, the rescaling of the membrane bead charges required a corresponding rescaling of electrostatic terms in the MM/PBSA calculations.

■ ASSOCIATED CONTENT

Supporting Information

The Supporting Information is available free of charge on the ACS Publications website at DOI: 10.1021/acschemneuro.8b00353.

Additional information on the behavior of Q17N17's side chains upon SUV titration, effects of titrating with different brain extract fractions, and representative examples of the MD trajectories with and without the model membrane (PDF)

N17Q17 in the absence of the model membrane (MPG)

N17Q17 in the presence of the model membrane (MPG)

■ AUTHOR INFORMATION

Corresponding Author

*E-mail: lucio.frydman@weizmann.ac.il. Phone: +972 8 934 4903.

ORCID

Yaakov Levy: 0000-0002-9929-973X

Lucio Frydman: 0000-0001-8208-3521

Present Addresses

∥K.S.: Department of Molecular and Cellular Biology, UC Berkeley, Berkeley, CA 94704, USA.

⊥P.E.S.S.: Florida State University/National High Magnetic Field Laboratory, Tallahassee, FL 32310, USA.

Author Contributions

G.R.L., K.S., R.C., Y.L., J.F., and L.F. designed research; G.R.L., K.S., Y.G. P.E.S.S., and R.C. acquired data and performed simulations; G.R.L., K.S., P.E.S.S., Y.G., Y.L., R.C., J.F., and L.F. contributed new tools and analyzed data; G.R.L., K.S., J.F., and L.F. wrote the paper.

Funding

This research was funded by the Israel Science Foundation Grant 965/18, by the I-CORE Program for the Planning and Budgeting Committee (ISF Grant 1775/12), by NIH Grant NS092525 (to J.F.), and by the generosity of the Perlman Family Foundation. P.E.S.S. is grateful for support from the National Institute on Aging (NIH) in the form of a National Research Service Award fellowship (1F32AG040957-01A1). K.S. was supported by a Stanford Graduate Fellowship.

Notes

The authors declare no competing financial interest.

■ ACKNOWLEDGMENTS

We thank Drs. Maria Baias and Tali Scherf for help in setting up the NMR experiments, and Dr. Gregory L. Olsen for valuable discussions.

■ ABBREVIATIONS

NMR, nuclear magnetic resonance; Htt, Huntingtin protein; N17Q17, seventeen amino acids N-terminal region of the Huntingtin protein followed by a polyglutamine chain of 17 residues; BEST, band-selective excitation short-transient H−N−C experiments; PSIPRED, protein structure prediction; SSP, secondary structure propensity; PONDR, predictors of natural disordered regions; VL-XT, Various methods to characterize Long disordered regions combined with Terminal disordered regions that were characterized using X-ray crystallography

■ REFERENCES

(1) Ross, C. A., Aylward, E. H., Wild, E. J., Langbehn, D. R., Long, J. D., Warner, J. H., Scahill, R. I., Leavitt, B. R., Stout, J. C., Paulsen, J. S., Reilmann, R., Unschuld, P. G., Wexler, A., Margolis, R. L., and Tabrizi, S. J. (2014) Huntington disease: natural history, biomarkers and prospects for therapeutics. *Nat. Rev. Neurol. 10* (4), 204−216.

(2) Orr, H. T., and Zoghbi, H. Y. (2007) Trinucleotide Repeat Disorders. *Annu. Rev. Neurosci. 30* (1), 575−621.

(3) Ross, C. A., and Poirier, M. A. (2004) Protein aggregation and neurodegenerative disease. *Nat. Med. 10* (7), S10−S17.

(4) Gauthier, L. R., Charrin, B. C., Borrell-Pagès, M., Dompierre, J. P., Rangone, H., Cordelières, F. P., De Mey, J., MacDonald, M. E., Lessmann, V., Humbert, S., and Saudou, F. (2004) Huntingtin controls neurotrophic support and survival of neurons by enhancing BDNF vesicular transport along microtubules. *Cell 118* (1), 127−138.

(5) Zuccato, C., Tartari, M., Crotti, A., Goffredo, D., Valenza, M., Conti, L., Cataudella, T., Leavitt, B. R., Hayden, M. R., Timmusk, T., Rigamonti, D., and Cattaneo, E. (2003) Huntingtin interacts with REST/NRSF to modulate the transcription of NRSE-controlled neuronal genes. *Nat. Genet. 35* (1), 76−83.

(6) Godin, J. D., Colombo, K., Molina-Calavita, M., Keryer, G., Zala, D., Charrin, B. C., Dietrich, P., Volvert, M.-L., Guillemot, F., Dragatsis, I., Bellaiche, Y., Saudou, F., Nguyen, L., and Humbert, S. (2010) Huntingtin is required for mitotic spindle orientation and mammalian neurogenesis. *Neuron 67* (3), 392−406.

(7) Molina-Calavita, M., Barnat, M., Elias, S., Aparicio, E., Piel, M., and Humbert, S. (2014) Mutant huntingtin affects cortical progenitor cell division and development of the mouse neocortex. *J. Neurosci. 34* (30), 10034−10040.

(8) Reiner, A., Dragatsis, I., Zeitlin, S., and Goldowitz, D. (2003) Wild-type huntingtin plays a role in brain development and neuronal survival. *Mol. Neurobiol. 28* (3), 259−276.

(9) MacDonald, M. (1993) A novel gene containing a trinucleotide repeat that is expanded and unstable on Huntington's disease chromosomes. *Cell 72* (6), 971−983.

(10) Scherzinger, E., Sittler, A., Schweiger, K., Heiser, V., Lurz, R., Hasenbank, R., Bates, G. P., Lehrach, H., and Wanker, E. E. (1999) Self-assembly of polyglutamine-containing huntingtin fragments into amyloid-like fibrils: implications for Huntington's disease pathology. *Proc. Natl. Acad. Sci. U. S. A. 96* (8), 4604−4609.

(11) Landles, C., Sathasivam, K., Weiss, A., Woodman, B., Moffitt, H., Finkbeiner, S., Sun, B., Gafni, J., Ellerby, L. M., Trottier, Y., Richards, W. G., Osmand, A., Paganetti, P., and Bates, G. P. (2010) Proteolysis of mutant huntingtin produces an exon 1 fragment that accumulates as an aggregated protein in neuronal nuclei in Huntington disease. *J. Biol. Chem. 285* (12), 8808−8823.

(12) Mangiarini, L., Sathasivam, K., Seller, M., Cozens, B., Harper, A., Hetherington, C., Lawton, M., Trottier, Y., Lehrach, H., Davies, S. W., and Bates, G. P. (1996) Exon 1 of the HD gene with an expanded CAG repeat is sufficient to cause a progressive neurological phenotype in transgenic mice. *Cell 87* (3), 493−506.

(13) Ratovitski, T., Gucek, M., Jiang, H., Chighladze, E., Waldron, E., D'Ambola, J., Hou, Z., Liang, Y., Poirier, M. A., Hirschhorn, R. R., Graham, R., Hayden, M. R., Cole, R. N., and Ross, C. A. (2009) Mutant Huntingtin N-terminal Fragments of Specific Size Mediate Aggregation and Toxicity in Neuronal Cells. *J. Biol. Chem. 284* (16), 10855−10867.

(14) Schilling, B., Gafni, J., Torcassi, C., Cong, X., Row, R. H., LaFevre-Bernt, M. A., Cusack, M. P., Ratovitski, T., Hirschhorn, R., Ross, C. A., Gibson, B. W., and Ellerby, L. M. (2006) Huntingtin

DOI: 10.1021/acschemneuro.8b00353
ACS Chem. Neurosci. 2019, 10, 472−481

phosphorylation sites mapped by mass spectrometry. Modulation of cleavage and toxicity. *J. Biol. Chem. 281* (33), 23686−23697.
(15) Jayaraman, M., Mishra, R., Kodali, R., Thakur, A. K., Koharudin, L. M. I., Gronenborn, A. M., and Wetzel, R. (2012) Kinetically competing huntingtin aggregation pathways control amyloid polymorphism and properties. *Biochemistry 51* (13), 2706−2716.
(16) Sivanandam, V. N., Jayaraman, M., Hoop, C. L., Kodali, R., Wetzel, R., and van der Wel, P. C. A. (2011) The aggregation-enhancing huntingtin N-terminus is helical in amyloid fibrils. *J. Am. Chem. Soc. 133* (12), 4558−4566.
(17) Williamson, T. E., Vitalis, A., Crick, S. L., and Pappu, R. V. (2010) Modulation of Polyglutamine Conformations and Dimer Formation by the N-Terminus of Huntingtin. *J. Mol. Biol. 396* (5), 1295−1309.
(18) Tam, S., Spiess, C., Auyeung, W., Joachimiak, L., Chen, B., Poirier, M. A., and Frydman, J. (2009) The chaperonin TRiC blocks a huntingtin sequence element that promotes the conformational switch to aggregation. *Nat. Struct. Mol. Biol. 16* (12), 1279−1285.
(19) Crick, S. L., Ruff, K. M., Garai, K., Frieden, C., and Pappu, R. V. (2013) Unmasking the roles of N- and C-terminal flanking sequences from exon 1 of huntingtin as modulators of polyglutamine aggregation. *Proc. Natl. Acad. Sci. U. S. A. 110* (50), 20075−80.
(20) Ruff, K. M., Khan, S. J., and Pappu, R. V. (2014) A coarse-grained model for polyglutamine aggregation modulated by amphipathic flanking sequences. *Biophys. J. 107* (5), 1226−35.
(21) Shen, K., Calamini, B., Fauerbach, J. A., Ma, B., Shahmoradian, S. H., Serrano Lachapel, I. L., Chiu, W., Lo, D. C., and Frydman, J. (2016) Control of the structural landscape and neuronal proteotoxicity of mutant Huntingtin by domains flanking the polyQ tract. *eLife 5*, 18065.
(22) Gu, X., Greiner, E. R., Mishra, R., Kodali, R., Osmand, A., Finkbeiner, S., Steffan, J. S., Thompson, L. M., Wetzel, R., and Yang, X. W. (2009) Serines 13 and 16 Are Critical Determinants of Full-Length Human Mutant Huntingtin Induced Disease Pathogenesis in HD Mice. *Neuron 64* (6), 828−840.
(23) Atwal, R. S., Desmond, C. R., Caron, N., Maiuri, T., Xia, J., Sipione, S., and Truant, R. (2011) Kinase inhibitors modulate huntingtin cell localization and toxicity. *Nat. Chem. Biol. 7* (7), 453−460.
(24) Thompson, L. M., Aiken, C. T., Kaltenbach, L. S., Agrawal, N., Illes, K., Khoshnan, A., Martinez-Vincente, M., Arrasate, M., O'Rourke, J. G., Khashwji, H., Lukacsovich, T., Zhu, Y. Z., Lau, A. L., Massey, A., Hayden, M. R., Zeitlin, S. O., Finkbeiner, S., Green, K. N., LaFerla, F. M., Bates, G., Huang, L., Patterson, P. H., Lo, D. C., Cuervo, A. M., Marsh, J. L., and Steffan, J. S. (2009) IKK phosphorylates Huntingtin and targets it for degradation by the proteasome and lysosome. *J. Cell Biol. 187* (7), 1083−99.
(25) Steffan, J. S. (2004) SUMO Modification of Huntingtin and Huntington's Disease Pathology. *Science 304* (5667), 100−104.
(26) Monsellier, E., Redeker, V., Ruiz-Arlandis, G., Bousset, L., and Melki, R. (2015) Molecular interaction between the chaperone Hsc70 and the N-terminal flank of huntingtin exon 1 modulates aggregation. *J. Biol. Chem. 290* (5), 2560−2576.
(27) Mishra, R., Hoop, C. L., Kodali, R., Sahoo, B., van der Wel, P. C. A., and Wetzel, R. (2012) Serine Phosphorylation Suppresses Huntingtin Amyloid Accumulation by Altering Protein Aggregation Properties. *J. Mol. Biol. 424* (1−2), 1−14.
(28) Mishra, R., Jayaraman, M., Roland, B. P., Landrum, E., Fullam, T., Kodali, R., Thakur, A. K., Arduini, I., and Wetzel, R. (2012) Inhibiting the Nucleation of Amyloid Structure in a Huntingtin Fragment by Targeting α-Helix-Rich Oligomeric Intermediates. *J. Mol. Biol. 415* (5), 900−917.
(29) Jayaraman, M., Kodali, R., Sahoo, B., Thakur, A. K., Mayasundari, A., Mishra, R., Peterson, C. B., and Wetzel, R. (2012) Slow Amyloid Nucleation via α-Helix-Rich Oligomeric Intermediates in Short Polyglutamine-Containing Huntingtin Fragments. *J. Mol. Biol. 415* (5), 881−899.
(30) Wetzel, R. Misfolding and Aggregation in Huntington Disease and Other Expanded Polyglutamine Repeat Diseases. In *Protein Misfolding Diseases*; John Wiley & Sons, Inc.: 2010; pp 305−324.
(31) Fiumara, F., Fioriti, L., Kandel, E. R., and Hendrickson, W. A. (2010) Essential Role of Coiled Coils for Aggregation and Activity of Q/N-Rich Prions and PolyQ Proteins. *Cell 143* (7), 1121−1135.
(32) Arrasate, M., Mitra, S., Schweitzer, E. S., Segal, M. R., and Finkbeiner, S. (2004) Inclusion body formation reduces levels of mutant huntingtin and the risk of neuronal death. *Nature 431* (7010), 805−810.
(33) Caron, N. S., Hung, C. L., Atwal, R. S., and Truant, R. (2014) Live cell imaging and biophotonic methods reveal two types of mutant huntingtin inclusions. *Hum. Mol. Genet. 23* (9), 2324−2338.
(34) Lu, J.-X., Qiang, W., Yau, W.-M., Schwieters, C. D., Meredith, S. C., and Tycko, R. (2013) Molecular Structure of & beta;-Amyloid Fibrils in Alzheimer's Disease Brain Tissue. *Cell 154* (6), 1257−1268.
(35) Slow, E. J., Graham, R. K., Osmand, A. P., Devon, R. S., Lu, G., Deng, Y., Pearson, J., Vaid, K., Bissada, N., Wetzel, R., Leavitt, B. R., and Hayden, M. R. (2005) Absence of behavioral abnormalities and neurodegeneration in vivo despite widespread neuronal huntingtin inclusions. *Proc. Natl. Acad. Sci. U. S. A. 102* (32), 11402−11407.
(36) Nagai, Y., Inui, T., Popiel, H. A., Fujikake, N., Hasegawa, K., Urade, Y., Goto, Y., Naiki, H., and Toda, T. (2007) A toxic monomeric conformer of the polyglutamine protein. *Nat. Struct. Mol. Biol. 14* (4), 332−340.
(37) Miller, J., Arrasate, M., Brooks, E., Libeu, C. P., Legleiter, J., Hatters, D., Curtis, J., Cheung, K., Krishnan, P., Mitra, S., Widjaja, K., Shaby, B. A., Lotz, G. P., Newhouse, Y., Mitchell, E. J., Osmand, A., Gray, M., Thulasiramin, V., Saudou, F., Segal, M., Yang, X. W., Masliah, E., Thompson, L. M., Muchowski, P. J., Weisgraber, K. H., and Finkbeiner, S. (2011) Identifying polyglutamine protein species in situ that best predict neurodegeneration. *Nat. Chem. Biol. 7* (12), 925−934.
(38) Nucifora, L. G., Burke, K. A., Feng, X., Arbez, N., Zhu, S., Miller, J., Yang, G., Ratovitski, T., Delannoy, M., Muchowski, P. J., Finkbeiner, S., Legleiter, J., Ross, C. A., and Poirier, M. A. (2012) Identification of novel potentially toxic oligomers formed in vitro from mammalian-derived expanded huntingtin exon-1 protein. *J. Biol. Chem. 287* (19), 16017−16028.
(39) Ceccon, A., Schmidt, T., Tugarinov, V., Kotler, S. A., Schwieters, C. D., and Clore, G. M. (2018) Interaction of Huntingtin Exon-1 Peptides with Lipid-Based Micellar Nanoparticles Probed by Solution NMR and Q-Band Pulsed EPR. *J. Am. Chem. Soc. 140* (20), 6199−6202.
(40) Baias, M., Smith, P. E., Shen, K., Joachimiak, L. A., Zerko, S., Kozminski, W., Frydman, J., and Frydman, L. (2017) Structure and Dynamics of the Huntingtin Exon-1 N-Terminus: A Solution NMR Perspective. *J. Am. Chem. Soc. 139*, 1168.
(41) Maget-Dana, R. (1999) The monolayer technique: a potent tool for studying the interfacial properties of antimicrobial and membrane-lytic peptides and their interactions with lipid membranes. *Biochim. Biophys. Acta, Biomembr. 1462* (1−2), 109−40.
(42) Bodner, C. R., Dobson, C. M., and Bax, A. (2009) Multiple tight phospholipid-binding modes of alpha-synuclein revealed by solution NMR spectroscopy. *J. Mol. Biol. 390* (4), 775−90.
(43) Louis-Jeune, C., Andrade-Navarro, M., and Perez-Iratxeta, C. (2012) Prediction of protein secondary structure from circular dichroism using theoretically derived spectra. *Proteins: Struct., Funct., Genet. 80* (2), 374−381.
(44) Cote, S., Binette, V., Salnikov, E. S., Bechinger, B., and Mousseau, N. (2015) Probing the Huntingtin 1−17 membrane anchor on a phospholipid bilayer by using all-atom simulations. *Biophys. J. 108* (5), 1187−98.
(45) Zhang, L., Kang, H., Vazquez, F. X., Toledo-Sherman, L., Luan, B., and Zhou, R. (2017) Molecular Mechanism of Stabilizing the Helical Structure of Huntingtin N17 in a Micellar Environment. *J. Phys. Chem. B 121* (18), 4713−4721.
(46) Thakur, A. K., Jayaraman, M., Mishra, R., Thakur, M., Chellgren, V. M., Byeon, I.-J. L., Anjum, D. H., Kodali, R.,

DOI: 10.1021/acschemneuro.8b00353
ACS Chem. Neurosci. 2019, 10, 472−481

Creamer, T. P., Conway, J. F., Gronenborn, A. M., and Wetzel, R. (2009) Polyglutamine disruption of the huntingtin exon 1 N terminus triggers a complex aggregation mechanism. *Nat. Struct. Mol. Biol. 16* (4), 380−389.
(47) Bauerlein, F. J. B., Saha, I., Mishra, A., Kalemanov, M., Martinez-Sanchez, A., Klein, R., Dudanova, I., Hipp, M. S., Hartl, F. U., Baumeister, W., and Fernandez-Busnadiego, R. (2017) In Situ Architecture and Cellular Interactions of PolyQ Inclusions. *Cell 171* (1), 179−187.e10.
(48) Orr, A. L., Li, S., Wang, C. E., Li, H., Wang, J., Rong, J., Xu, X., Mastroberardino, P. G., Greenamyre, J. T., and Li, X. J. (2008) N-terminal mutant huntingtin associates with mitochondria and impairs mitochondrial trafficking. *J. Neurosci. 28* (11), 2783−92.
(49) Rockabrand, E., Slepko, N., Pantalone, A., Nukala, V. N., Kazantsev, A., Marsh, J. L., Sullivan, P. G., Steffan, J. S., Sensi, S. L., and Thompson, L. M. (2007) The first 17 amino acids of Huntingtin modulate its sub-cellular localization, aggregation and effects on calcium homeostasis. *Hum. Mol. Genet. 16* (1), 61−77.
(50) Rui, Y. N., Xu, Z., Patel, B., Chen, Z., Chen, D., Tito, A., David, G., Sun, Y., Stimming, E. F., Bellen, H. J., Cuervo, A. M., and Zhang, S. (2015) Huntingtin functions as a scaffold for selective macroautophagy. *Nat. Cell Biol. 17* (3), 262−75.
(51) Burke, K. A., Hensal, K. M., Umbaugh, C. S., Chaibva, M., and Legleiter, J. (2013) Huntingtin disrupts lipid bilayers in a polyQ-length dependent manner. *Biochim. Biophys. Acta, Biomembr. 1828* (8), 1953−61.
(52) Kegel-Gleason, K. B. (2013) Huntingtin interactions with membrane phospholipids: Strategic targets for therapeutic intervention? *J. Huntington's Dis. 2* (3), 239−50.
(53) Michalek, M., Aisenbrey, C., and Bechinger, B. (2014) Investigation of membrane penetration depth and interactions of the amino-terminal domain of huntingtin: refined analysis by tryptophan fluorescence measurement. *Eur. Biophys. J. 43* (8−9), 347−60.
(54) Michalek, M., Salnikov, E. S., and Bechinger, B. (2013) Structure and topology of the huntingtin 1−17 membrane anchor by a combined solution and solid-state NMR approach. *Biophys. J. 105* (3), 699−710.
(55) Pandey, N. K., Isas, J. M., Rawat, A., Lee, R. V., Langen, J., Pandey, P., and Langen, R. (2018) The 17-residue-long N terminus in huntingtin controls stepwise aggregation in solution and on membranes via different mechanisms. *J. Biol. Chem. 293* (7), 2597−2605.
(56) Michalek, M., Salnikov, E. S., and Bechinger, B. (2013) Structure and Topology of the Huntingtin 1−17 Membrane Anchor by a Combined Solution and Solid-State NMR Approach. *Biophys. J. 105* (3), 699−710.
(57) Binette, V., Cote, S., and Mousseau, N. (2016) Free-Energy Landscape of the Amino-Terminal Fragment of Huntingtin in Aqueous Solution. *Biophys. J. 110* (5), 1075−88.
(58) Burke, K. A., Kauffman, K. J., Umbaugh, C. S., Frey, S. L., and Legleiter, J. (2013) The interaction of polyglutamine peptides with lipid membranes is regulated by flanking sequences associated with huntingtin. *J. Biol. Chem. 288* (21), 14993−5005.
(59) Nagarajan, A., Jawahery, S., and Matysiak, S. (2014) The effects of flanking sequences in the interaction of polyglutamine peptides with a membrane bilayer. *J. Phys. Chem. B 118* (24), 6368−79.
(60) Atwal, R. S., Desmond, C. R., Caron, N., Maiuri, T., Xia, J., Sipione, S., and Truant, R. (2011) Kinase inhibitors modulate huntingtin cell localization and toxicity. *Nat. Chem. Biol. 7* (7), 453−60.
(61) Kokona, B., Rosenthal, Z. P., and Fairman, R. (2014) Role of the Coiled-Coil Structural Motif in Polyglutamine Aggregation. *Biochemistry 53* (43), 6738−6746.
(62) Kokona, B., Johnson, K. A., and Fairman, R. (2014) Effect of Helical Flanking Sequences on the Morphology of Polyglutamine-Containing Fibrils. *Biochemistry 53* (43), 6747−6753.
(63) Chaibva, M., Jawahery, S., Pilkington, A. W. t., Arndt, J. R., Sarver, O., Valentine, S., Matysiak, S., and Legleiter, J. (2016) Acetylation within the First 17 Residues of Huntingtin Exon 1 Alters Aggregation and Lipid Binding. *Biophys. J. 111* (2), 349−362.
(64) Grey, M., Dunning, C. J., Gaspar, R., Grey, C., Brundin, P., Sparr, E., and Linse, S. (2015) Acceleration of alpha-synuclein aggregation by exosomes. *J. Biol. Chem. 290* (5), 2969−82.
(65) Alberts, B, Johnson, A., Lewis, J., Raff, M., Roberts, K., and Walter, P. Fractionation of Cells. In *Molecular Biology of the Cell*, 4th ed.; Garland Science: New York, 2002.
(66) Schanda, P., Van Melckebeke, H., and Brutscher, B. (2006) Speeding up three-dimensional protein NMR experiments to a few minutes. *J. Am. Chem. Soc. 128* (28), 9042−3.
(67) Delaglio, F., Grzesiek, S., Vuister, G., Zhu, G., Pfeifer, J., and Bax, A. (1995) NMRPipe: A multidimensional spectral processing system based on UNIX pipes. *J. Biomol. NMR 6* (3), 277−293.
(68) Foloppe, N., and MacKerell, A. D., Jr. (2000) All-atom empirical force field for nucleic acids: I. Parameter optimization based on small molecule and condensed phase macromolecular target data. *J. Comput. Chem. 21* (2), 86−104.
(69) MacKerell, A. D., and Banavali, N. K. (2000) All-atom empirical force field for nucleic acids: II. Application to molecular dynamics simulations of DNA and RNA in solution. *J. Comput. Chem. 21* (2), 105−120.
(70) MacKerell, A. D., Bashford, D., Bellott, M., Dunbrack, R. L., Evanseck, J. D., Field, M. J., Fischer, S., Gao, J., Guo, H., Ha, S., Joseph-McCarthy, D., Kuchnir, L., Kuczera, K., Lau, F. T., Mattos, C., Michnick, S., Ngo, T., Nguyen, D. T., Prodhom, B., Reiher, W. E., Roux, B., Schlenkrich, M., Smith, J. C., Stote, R., Straub, J., Watanabe, M., Wiorkiewicz-Kuczera, J., Yin, D., and Karplus, M. (1998) All-atom empirical potential for molecular modeling and dynamics studies of proteins. *J. Phys. Chem. B 102* (18), 3586−616.
(71) Mackerell, A. D., Jr., Feig, M., and Brooks, C. L., 3rd (2004) Extending the treatment of backbone energetics in protein force fields: limitations of gas-phase quantum mechanics in reproducing protein conformational distributions in molecular dynamics simulations. *J. Comput. Chem. 25* (11), 1400−15.
(72) Hess, B., Bekker, H., Berendsen, H. J. C., and Fraaije, J. G. E. M. (1997) LINCS: A linear constraint solver for molecular simulations. *J. Comput. Chem. 18* (12), 1463−1472.
(73) Bussi, G., Donadio, D., and Parrinello, M. (2007) Canonical sampling through velocity rescaling. *J. Chem. Phys. 126* (1), 014101.
(74) Mark, P., and Nilsson, L. (2001) Structure and dynamics of the TIP3P, SPC, and SPC/E water models at 298 K. *J. Phys. Chem. A 105* (43), 9954−9960.
(75) Marchi, M., Sterpone, F., and Ceccarelli, M. (2002) Water rotational relaxation and diffusion in hydrated lysozyme. *J. Am. Chem. Soc. 124* (23), 6787−91.
(76) *The PyMOL Molecular Graphics System*, Version 1.7.0.5; Schrödinger LLC, 2015.
(77) Kumari, R., Kumar, R., Open Source Drug Discovery Consortium, and Lynn, A. (2014) g_mmpbsa-A GROMACS Tool for High-Throughput MM-PBSA Calculations. *J. Chem. Inf. Model. 54* (7), 1951−1962.

DOI: 10.1021/acschemneuro.8b00353
ACS Chem. Neurosci. 2019, 10, 472−481